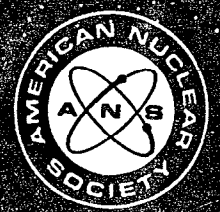




# NUCLEAR SCIENCE and ENGINEERING



# Dynamic Subcriticality Measurements Using the <sup>252</sup>Cf-Source-Driven Noise Analysis Method

J. T. Mihalcz, E. D. Blakeman, G. E. Ragan, and E. B. Johnson  
Oak Ridge National Laboratory, Instrumentation and Controls Division  
Oak Ridge, Tennessee 37831-6305

and

Y. Hachiya  
Power Reactor and Nuclear Fuel Development Corporation, Tokyo, Japan

Received January 18, 1989  
Accepted September 22, 1989

**Abstract**—Dynamic measurements of the subcritical neutron multiplication factor  $k_{eff}$  using the <sup>252</sup>Cf-source-driven neutron noise analysis method were performed for an unreflected 25.1-cm-i.d. cylindrical tank containing aqueous uranyl nitrate as the solution height was changed at rates of 1 to 23 cm/min, with corresponding changes in  $k_{eff}$  from  $4 \times 10^{-4}$  to 0.01/s.

These experiments, which were the first test of the method to measure  $k_{eff}$  while it is changing, showed the following:

1. This method has the capability to measure subcriticality for a multiplying system to a  $k_{eff}$  as low as 0.30.
2. Experimental  $k_{eff}$  values can be obtained from the ratio of spectral densities with as little as 6 s of data accumulation and a small fraction of a second analysis time while the solution tank is drained from a height of 29.5 to 6.5 cm in ~60 s, with corresponding changes in  $k_{eff}$  from 0.95 to 0.30.
3. The measured  $k_{eff}$  values obtained do not depend on the speed at which the solution height is changed or whether it is filling or draining.
4. The results of the dynamic measurements agreed with the static measurements.
5. Where static measurements were practical (limited to  $k_{eff}$  down to ~0.5 by detection efficiency) with <sup>3</sup>He proportional counters sensitive to leakage neutrons only, the results agreed with those from measurements with scintillation detectors sensitive to gamma rays and neutrons escaping from the system.
6. As in previous experiments, the ratios of spectral densities at low frequency were used successfully to obtain  $k_{eff}$  values using a modified point kinetics interpretation of the data.
7. The neutron multiplication factors from independent measurements using the break frequency noise analysis method agree with the values of  $k_{eff}$  from the measured ratios of spectral densities down to  $k_{eff}$  values of 0.65.
8. The effectiveness of this method for systems where conditions are changing probably exceeds the dynamic requirements of most nuclear fuel plant processing applications.
9. Calculated  $k_{eff}$  values using the KENO Monte Carlo code and Hansen-Roach cross sections compare well with the experimental values.

compressed through four 0.63-cm-diam threaded steel tie rods, equally spaced around the circumference of the vessel, joining the base and a stainless steel upper flange. A 0.63-cm-thick, 32- × 32-cm square acrylic plate on top of the upper flange provided access for the source and minimized evaporation of the solution.

The height of solution above the base plate was determined by an ultrasonic device with a transducer mounted on the acrylic cover of the vessel over a circular opening. Every 0.125 s, this device sampled and stored in the computer the solution height to within  $\pm 0.2$  mm. Figure 1 is a photograph of the experimental vessel showing the mounted transducer and the  $^{252}\text{Cf}$  source ionization chamber at the top of the solution.

The vessel was mounted on a 122- × 122-cm square aluminum table 76 cm above a steel grating covered with a stainless steel sheet. This grating was 3.6 m above the concrete floor of the experiment cell. The cell in which the equipment was assembled was  $\sim 9.1 \times 12.2 \times 9.1$  m high with thick concrete walls and roof. The experiment vessel was located 4.4 m from the 9.1-m south side of the cell, 3.0 m from the 12.2-m east side, and  $\sim 1.85$  m from a 2.9-m-diam empty steel tank (2.5 cm thick) also present in the cell. The steel tank

was located in the cell such that its axis was 4 m from the 9.1-m south side of the cell and 6.2 m from the 12.2-m east side.

The aqueous uranyl nitrate contained and a solution density of  $1.643 \text{ g/cm}^3$ , with content  $< 0.1 \text{ wt}\%$   $\text{HNO}_3$ . Uranium isotopes were  $^{234}\text{U} = 1.02$ ,  $^{235}\text{U} = 93.2$ ,  $^{236}\text{U} = 0.41$ , and  $^{238}\text{U} = 5.37 \text{ wt}\%$  and was free of significant impurities.

The  $^{252}\text{Cf}$  was electroplated on one parallel-plate ionization chamber, and the spallation rate was  $60\,000/\text{s}$  ( $\sim 0.1 \mu\text{g } ^{252}\text{Cf}$ ). The ionization chamber was mounted at the end of a 1.27-cm-i.d. Lexan tube with the source from the chamber inside the Lexan tube (the source was sealed from the solution with stainless steel and epoxy). The Lexan tubing and the signal wires protruded out the top of the solution through a hole in the lid of the experimental vessel. The source could be located anywhere along the axis of the cylindrical experimental vessel. In most of the experiments, the source was located at the bottom of the experimental vessel. In practical applications of cylindrical tanks, the bottom of the tank is a convenient location for the source. For measurements at various solution heights, the source was located on the axis at the vertical mid-height of the solution, but in some measurements, its position on the axis was varied.

Two types of detectors were used in the experiments: commercially available  $^3\text{He}$  proportional counters primarily for static measurements and an assembled composite  $^6\text{Li}$ -glass organic scintillator for both static and dynamic measurements. The  $^6\text{Li}$ -glass organic scintillator was a proportional counter (5.1-cm-diam, 38-cm-long, Reuter-Stokes model RS-P4-1641-101) with their axes parallel to the axis of the vessel adjacent to the outer surface of the vessel on the east and west sides, 180 deg apart azimuthally. They detected leakage neutrons. One end of the detector was at the bottom of the tank. Thus, as the solution height changed, the active length of the detector was essentially the height of the solution. Two such detectors on the east and west sides of the tank were present for the dynamic measurements.

The scintillation detectors were composed of glass organic scintillators sensitive to fast neutrons and gamma rays. Each scintillator consisted of a  $15.2 \times 15.2 \times 0.5$ -cm-thick glass scintillator optically coupled to a  $15.2 \times 15.2 \times 10.7$ -cm-thick organic scintillator sensitive to fast neutrons and gamma rays. The  $^6\text{Li}$ -glass scintillator was placed adjacent to the experimental vessel with the organic scintillator inside it so that the organic was almost neutrally moderated by the solution by the absorption of neutrons in the  $^6\text{Li}$ . Each detection channel consisted of two adjacent  $15.2 \times 15.2 \times 10.7$ -cm-thick scintillators, each mounted in an aluminum box (with a lead wall) that formed a detection channel.

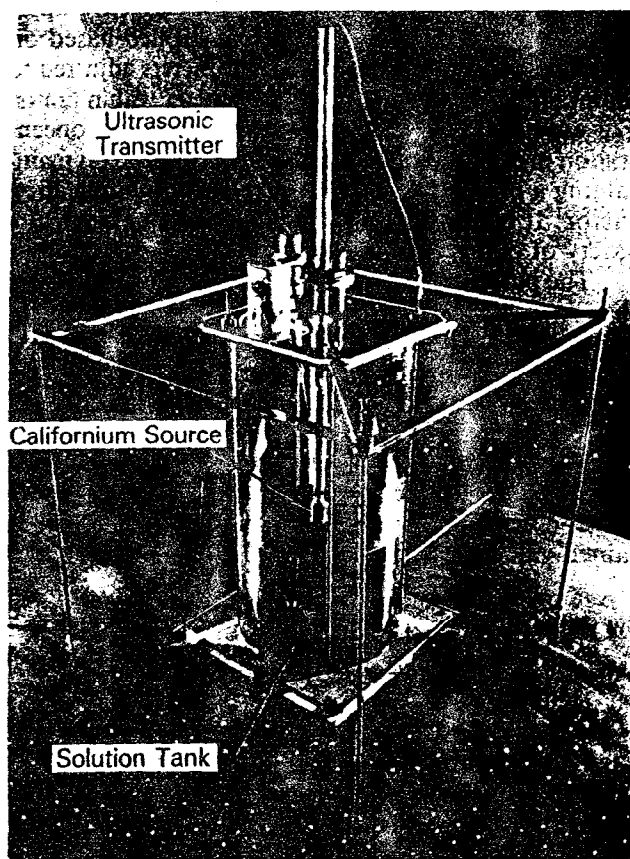


Fig. 1. The experimental vessel.

with time is compared with the results of measurements where the solution height was fixed. For these comparisons, the neutron multiplication factor obtained for the average height in the dynamic measurements was compared with static measurements fixed at the average height. The results are also compared with those from break frequency noise analysis measurements.

### STATIC MEASUREMENTS

Static measurements were performed to obtain reference measurements to compare with the results of dynamic measurements. These measurements were performed as a function of solution height with the  $^{252}\text{Cf}$  source located on the axis at the center of the solution. In the static measurements, the detectors were  $^3\text{He}$  proportional counters 180 deg apart, adjacent to the outer surface of the vessel with their axes parallel to the

axis of the experimental vessel and  $^6\text{Li}$ -glass organic scintillators located as shown in Fig. 2. The length of the  $^3\text{He}$  detectors was more than the height of the solution.

Typical ratios of spectral densities as a function of frequency are shown in Fig. 3. These ratios were examined visually to determine the range of frequencies over which the ratio of spectral densities was constant. This range of frequencies is generally greater for more subcritical systems because the frequency response of the experimental system  $H_s(\omega)$  has significant amplitude at higher frequency. The range of frequencies over which the ratio was arithmetically averaged was then selected to eliminate high-frequency points for which the statistical uncertainty was large and would lead to high or low values of the ratio that would distort the average value of the ratio. Thus, both of these criteria, constant ratio and small

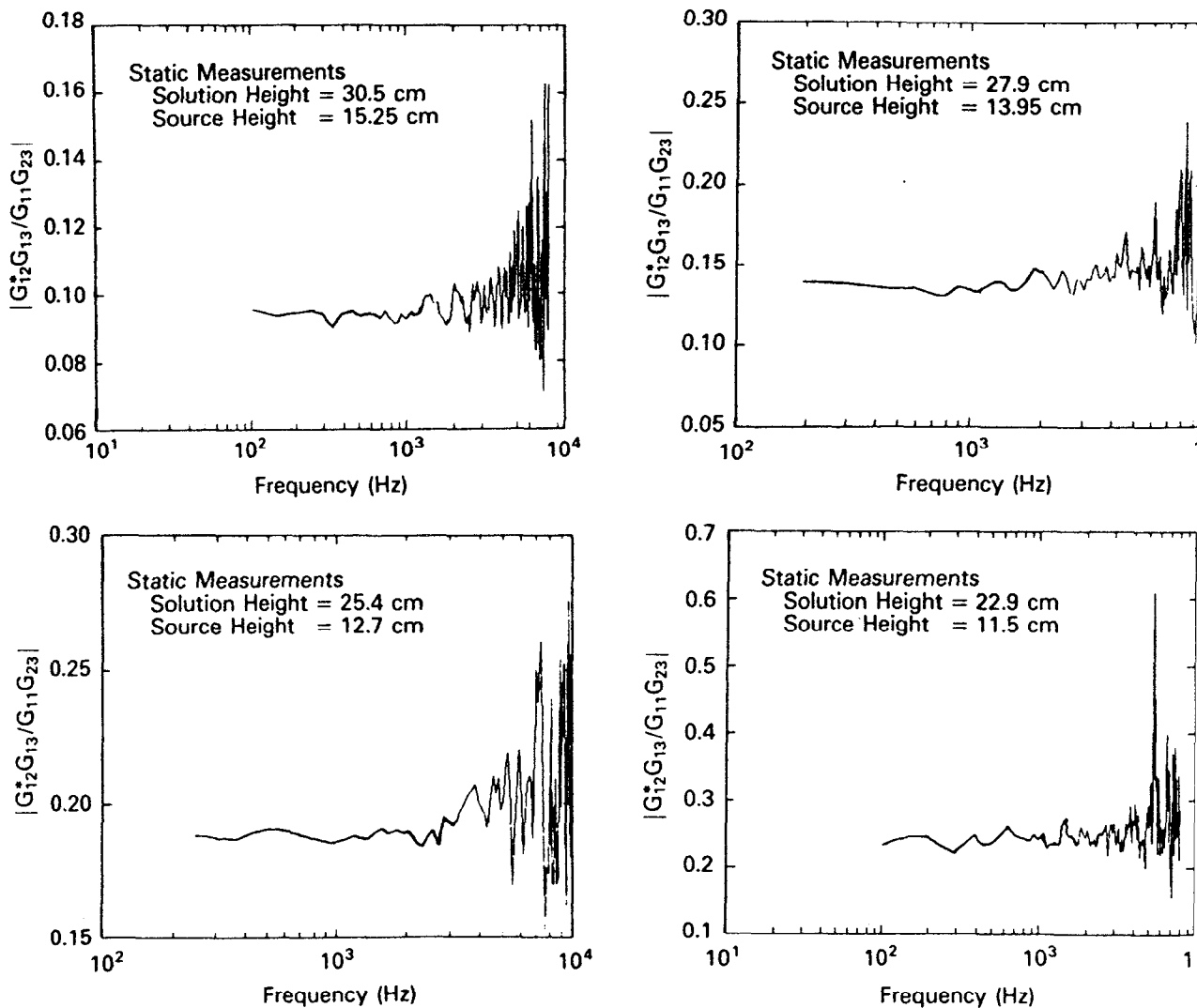


Fig. 3. Ratios of spectral densities as a function of frequency for vari

TABLE I

Ratios of Spectral Densities  $G_{12}^*G_{13}/G_{11}G_{23}$  at Low Frequency for Various Solution Heights from Static Measurements with Central Source and  $^3\text{He}$  Proportional Counters Adjacent to the Outer Surface of the Experimental Vessel

Solution Height (cm)	Bandwidth of Measurement (kHz)	Number of Data Samples ( $10^3$ )	Ratios of Spectral Densities <sup>a</sup> ( $10^{-3}$ )	Upper Limit of Frequency Range for Ratio (kHz)	Neutron Multiplication Factor	
					Measurement	Calculation
30.5	20	80	$100 \pm 1$	3	0.963	0.950
30.5	40	80	$96 \pm 1$	3	0.964	---
27.9	40	80	$139 \pm 1$	3	0.945	0.916
25.4	50	240	$190 \pm 1$	3	0.919	0.896
22.9	20	40	$248 \pm 3$	5	0.884	0.870
20.3	100	160	$304 \pm 3$	8	0.843	0.831
20.3	100	40	$303 \pm 5$	7	0.843	---
15.2	50	840	$465 \pm 3$	5	0.704	0.721
10.2	100	9360	$525^c$	$0.4^c$	0.570	0.547

<sup>a</sup>Uncertainties are one standard deviation of the mean.

<sup>b</sup>Monte Carlo calculations using Hansen-Roach cross sections with the effects of source materials included.

<sup>c</sup>For this measurement, the ratio of spectral densities was not constant at low frequencies (Fig. 3), so the value measured at 400 Hz was used to obtain the neutron multiplication factor.

were performed using KENO Monte Carlo calculations with Hansen-Roach cross sections (Table C.I in Appendix C provides details of calculations).

Static measurements were also performed with the source at the bottom of the solution with both  $^6\text{Li}$ -

glass organic scintillators and  $^3\text{He}$  detectors. The ratios of spectral densities at low frequency for both types of detectors are given in Table II. For low solution heights (<10 cm), statistically meaningful measurements with the  $^3\text{He}$  proportional counters were

TABLE II

Ratios of Spectral Densities at Low Frequency and Neutron Multiplication Factors from Static Measurements with the Source at the Bottom of the Solution

Solution Height (cm)	Ratio of Spectral Densities <sup>a</sup>		Neutron Multiplication Factors, $k_{eff}^b$		Number of Data Blocks ( $10^3$ )
	$^3\text{He}$ Detectors ( $10^{-4}$ )	Scintillators ( $10^{-4}$ )			
			$^3\text{He}$ Detectors	Scintillators	
29.2	$453 \pm 12$ (5)	$436 \pm 5$ (2)	$0.952 \pm 0.002$	$0.954 \pm 0.001$	20
25.8	$767 \pm 40$ (5)	$774 \pm 20$ (2)	$0.924 \pm 0.005$	$0.923 \pm 0.003$	20
20.3	$1590 \pm 20$ (5)	$1616 \pm 10$ (6)	$0.853 \pm 0.005$	$0.850 \pm 0.005$	20
15.3	$2896 \pm 90$ (5)	$2843 \pm 10$ (10)	$0.732 \pm 0.015$	$0.738 \pm 0.010$	40
10.1	$4508 \pm 90$ (5)	$4477 \pm 60$ (10)	$0.535 \pm 0.030$	$0.540 \pm 0.027$	20
9.8	---	$4723 \pm 60$ (10)	---	$0.505 \pm 0.030$	7
9.0	---	$4960 \pm 60$ (10)	---	$0.472 \pm 0.035$	100
7.5	---	$5293 \pm 210$ (10)	---	$0.414 \pm 0.055$	40
6.5	---	$5650 \pm 60$ (10)	---	$0.346 \pm 0.049$	60
5.7	---	$5943 \pm 360$ (10)	---	$0.278 \pm 0.097$	55

<sup>a</sup>Values in parentheses are the upper limit of the frequency range in kilohertz over which the ratio was averaged. The precision given is one standard deviation of the mean.

<sup>b</sup>Uncertainties are statistical precision of the ratio of spectral densities and uncertainties in the parameters of Appendix B. The largest contribution to the uncertainty was from  $I_c/I$  (e.g., 80% of the uncertainty for a solution height 6.5 cm). All tables in this paper other than Tables II and III have uncertainties from the precision of the ratio of spectral densities only.



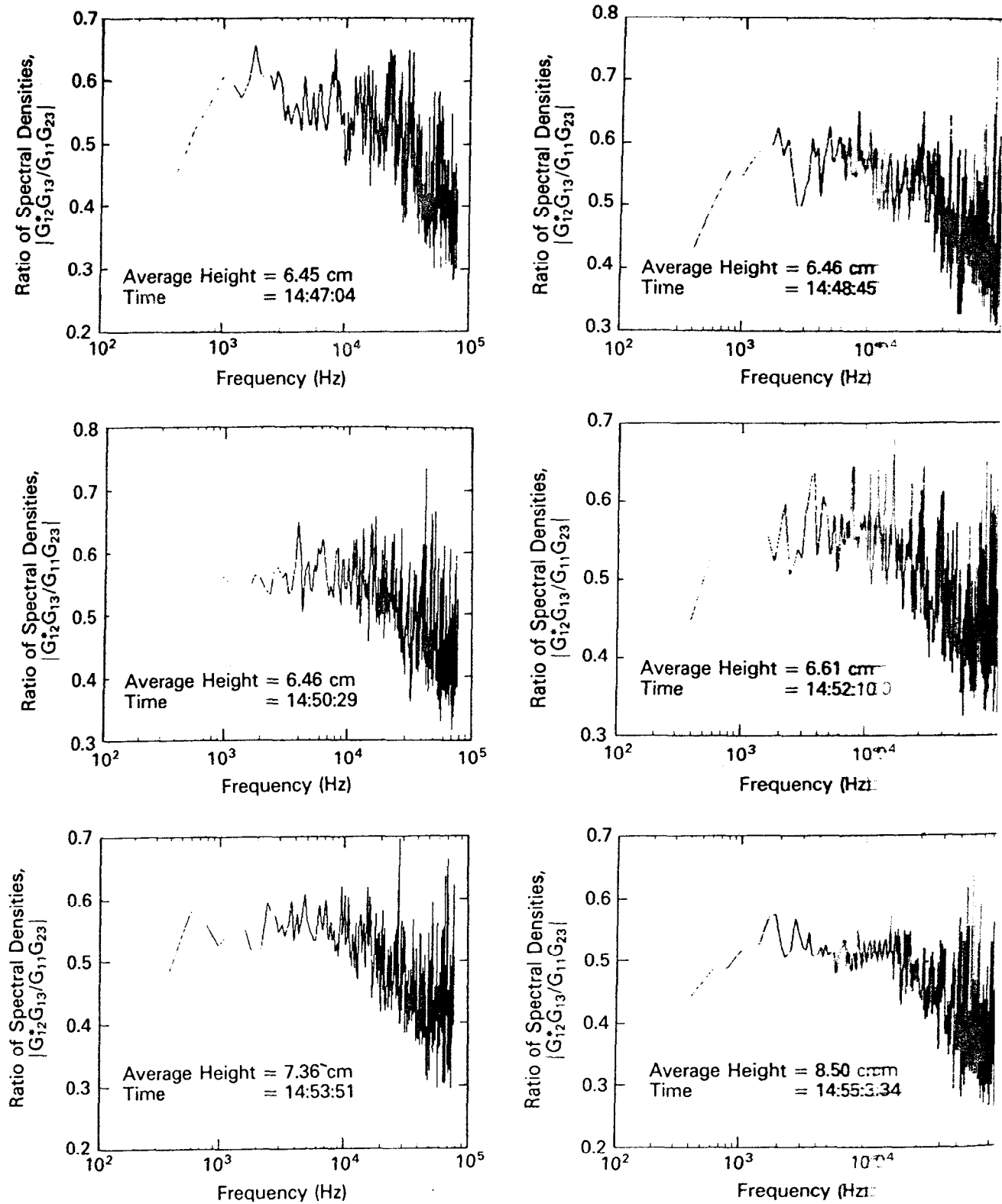


Fig. 5. Ratios of spectral densities as a function of frequency as the experimental vessel was filled at a rate of 1 cm/ (continued on following pages).

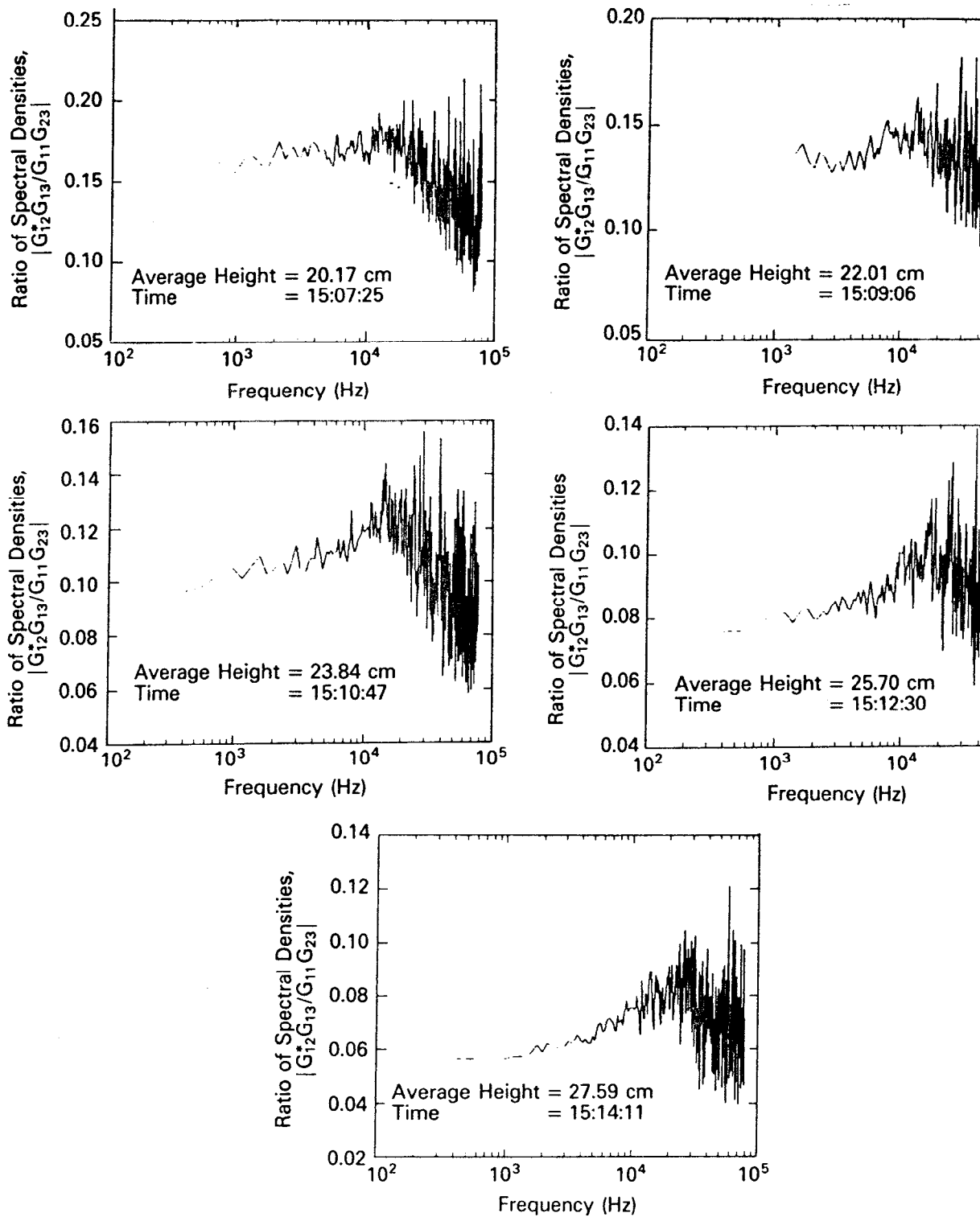
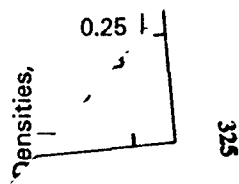


Fig. 5. (Continued)

in the measured neutron multiplication factor varies from 0.01 at the lowest  $k_{eff}$  ( $\sim 0.31$ ) to  $< 0.001$  at higher  $k_{eff}$  values (0.93).

The first three entries of Table III are for the same

solution height. Intercomparison of these three measurements (102 s of data accumulation time) show the ratios and the resulting neutron multiplication factors are reproducible even at  $k_{eff}$  values as



coherence values and short coherence at low frequency. The channel and the californium source and the two scintillator channels as a function of solution height at low frequency at the bottom are  $\gamma_{12}^2 = 0.045$  and solution height of 27.6 cm. As in previous measurements,  $k_{eff}$  is a function of subcritical-

Fig. 7-23.

The experimental vessel was drained at three different rates with the source on the bottom of the tank. The fastest rate was such that the height varied from 29.5 to ~6 cm in ~60 s. This limit on the draining rate resulted from the 1.27-cm-diam opening in the bottom of the tank. Other draining rates were such that the height of solution changed 3 and 5 cm/min.

For a draining rate corresponding to a change of solution height of ~3 cm/min, the data accumulation time before the Fourier processor uploaded the data to the VAX computer for interpretation was ~13 s while that for more rapid draining of the tank (5 and 23 cm/min) was 6.4 s. Thus, these data have a larger statistical error than data for filling the experimental vessel because the data accumulation time is a factor of 8 to 16 shorter. The ratios of spectral densities at low frequency for their draining rates are plotted as a function of solution height in Fig. 6. The  $k_{eff}$  values obtained from these measurements are in agreement with those from filling the vessel (Fig. 7).

For a draining rate that corresponds to a change in solution height of 23 cm/min ( $\Delta k_{eff}/s \approx 0.01$ ), the solution was drained continuously from 28.9 to 5.7 cm.

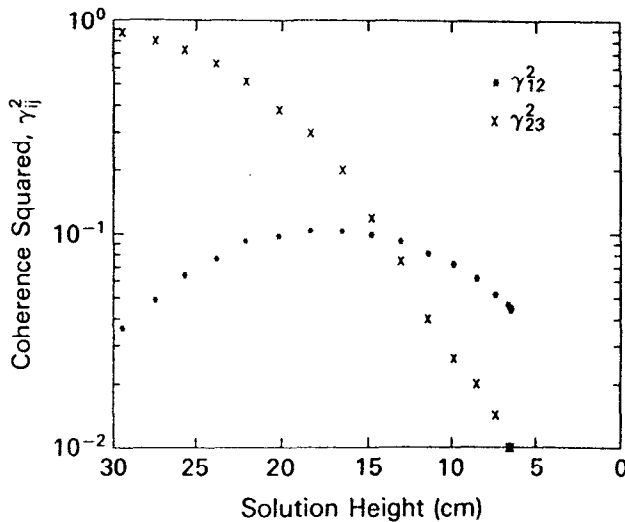


Fig. 8. Coherence squared,  $\gamma_{12}^2$  and  $\gamma_{23}^2$ , at low frequency as a function of solution height for experiments with the californium source at the bottom of the solution and with scintillation detectors.

The draining rate was limited by the size of the hole (1.27 cm) provided in the bottom of the tank. The results of the data interpretation are given in Table IV. The precision of the measured ratio of spectral densities is such that the precision in the  $k_{eff}$  value is (down to ~0.60 (solution height of 12 cm) for the collection time of 6.4 s and the draining rate of 23 cm/min. For the last four entries of Table IV, the solution height was fixed at 5.72 cm and the average  $k_{eff}$  value obtained is 0.30. The ratios of spectral densities and neutron multiplication factors are plotted as a function of solution height in Figs. 5 and 6, where they are compared with the other dynamic measurements.

The rate of change of the neutron multiplication factor in this experiment was 0.01 in  $k_{eff}$  per second. The neutron multiplication factor from all dynamic measurements (filling at a rate of 1 cm/min and draining at rates of 3, 5, and 23 cm/min) and the static measurements are in agreement. Thus, over the range of filling and draining rates investigated, the  $k_{eff}$  values measured do not depend on the rate of change of  $k_{eff}$  or whether the solution height is increased, decreased, or stationary. The dynamic capability of the method may be more than that required for most nuclear processing or reprocessing plant applications.

#### Solution Perturbed by Bubbles

After the experimental vessel was filled to 29.5 cm, exploratory experiments were performed with air bubbles introduced into the bottom of the tank by the pump running with no fuel solution in the tank. As a result, air was continuously added to the bottom of the tank through a 1.3-cm-diam hole at a radius of 7.6 cm. Air bubbles moved vertically through the solution, displacing fuel solution from the interior of the solution tank and also perturbing the upper surface of the solution. This displacement of fuel solution from the interior to the upper surface decreased the activity. For this measurement, the source was on the x-axis at the bottom of the tank.

These exploratory experiments were the first experiments in which a solution was perturbed during this type of measurement (a perturbed solution tank is typical of some tanks in in-plant applications). Since these were exploratory measurements, no quantitative characterization of the bubbling was performed other than the estimate that the volume of air continuously introduced into the solution was ~500 cm<sup>3</sup>/min. The data accumulation rates were such that 102 s of data were accumulated by the Fourier analyzer before the data file was uploaded to the VAX computer.

The ratios of spectral densities at low frequency with and without bubbles are given in Table V along with the  $k_{eff}$  values obtained using the same parameters with and without bubbles. The assumption that the same parameters can be used is probably valid since the air introduction was not a large perturbation.



associated with the bubbles is a small decrease ( $\sim 1.6 \times 10^{-3}$ ).

### BREAK FREQUENCY NOISE ANALYSIS METHOD

The break frequency noise analysis (BFNA) method provides another technique for measuring the subcritical neutron multiplication factor and thus can be compared to the results of the californium-source-driven noise analysis method. It is not completely independent of the californium-source-driven noise method since the BFNA method uses a reference reactivity of  $k_{eff} \approx 0.95$  measured by the californium method.

The various spectral densities as a function of frequency can be least-squares fitted to obtain the fundamental mode break frequency  $f_b$ . The reactivity at a given subcritical state is related to the fundamental mode break frequency at that subcritical state  $f_b$  (or to the prompt neutron decay constant  $\alpha = 2\pi f_b$ ) and to the fundamental mode break frequency at delayed criticality  $f_{bdc}$  (or prompt neutron decay constant  $\alpha_{dc} = \beta/l$ ) as follows<sup>13</sup>:

$$\frac{\alpha}{\alpha_{dc}} = \frac{f_b}{f_{bdc}} = \frac{1 - k_{eff}}{k_{eff}\beta} + 1.$$

Equation (1) must be corrected for the changes in the neutron lifetime and in the effective delayed neutron fraction from the delayed critical state to the subcritical state of interest as follows:

$$\frac{1 - k_{eff}}{k_{eff}\beta} + 1 = \frac{f_b}{f_{bdc}} \frac{l}{l_{dc}} \frac{\beta_{dc}}{\beta}.$$

For the reactivity changes in these experiments corrections for neutron lifetime and effective delayed neutron fraction changes were made. The ratios of prompt neutron lifetimes and the ratios of effective delayed neutron fractions were obtained from calculations of these quantities as a function of solution height, which used fixed source forward fluxes and  $k_{eff}$  eigenvalues adjoint fluxes from  $S_8$  transport theoretical calculations.

The break frequency for each solution height was obtained by fitting the various CPSDs and APSDs as functions of frequency  $\omega$  to functional forms with (a) a single pole in the transfer function [ $H(\omega)$ ]

TABLE VI

Break Frequencies Obtained from Least-Squares Fitting of APSDs and CPSDs and Neutron Multiplication Factors from the BFNA Method as a Function of Solution Height

Solution Height (cm)	Fundamental Mode Break Frequency ( $s^{-1}$ )		Percentage Change in $\frac{l\beta_{dc}}{dc\beta}$	Reactivity from BFNA ( $\beta$ )	$k_{eff}$	
	One Mode	Two Mode			BFNA	Ratio of Spectral Densities <sup>a</sup>
29.5	1369 ± 7 <sup>b</sup>	1328 ± 12	0	6.13 <sup>c</sup>	0.956 <sup>d</sup> ± 0.003	0.956 <sup>c</sup> ± 0.001
29.5	1385 ± 7	1357 ± 24	0	6.13 <sup>c</sup>	0.956 <sup>d</sup> ± 0.003	0.956 <sup>c</sup> ± 0.001
29.5	1375 ± 7	1336 ± 16	0	6.13 <sup>c</sup>	0.956 <sup>d</sup> ± 0.003	0.956 <sup>c</sup> ± 0.001
27.6	1819 ± 13	1776 ± 21	1.1	8.6	0.939 ± 0.004	0.940 ± 0.002
25.7	2320 ± 9	2265 ± 15	2.4	11.3	0.921 ± 0.004	0.921 ± 0.002
23.8	2889 ± 12	2850 ± 15	3.7	14.7	0.899 ± 0.005	0.896 ± 0.003
22.0	3563 ± 14	3503 ± 18	5.3	18.6	0.875 ± 0.006	0.872 ± 0.004
20.2	4327 ± 8	4308 ± 30	6.5	23.4	0.845 ± 0.007	0.845 ± 0.005
18.4	5175 ± 20	5117 ± 36	9.7	28.8	0.814 ± 0.009	0.812 ± 0.006
16.5	6218 ± 13	6280 ± 75	13.5	36.9	0.772 ± 0.010	0.771 ± 0.008
14.7	7468 ± 18	7760 ± 85	18.5	47.9	0.720 ± 0.011	0.723 ± 0.011
13.1	8955 ± 30	9629 ± 164	24.6	62.8	0.659 ± 0.013	0.662 ± 0.015
11.4	10537 ± 31	11196 ± 313	32.3	77.8	0.605 ± 0.009	0.588 ± 0.021
9.9	12325 ± 98	12849 ± 75	44.3	97.7	0.543 ± 0.014	0.522 ± 0.027
8.5	14388 ± 143	14825 ± 100	56.1	122.2	0.478 ± 0.014	0.443 ± 0.038
7.3	16414 ± 197	16750 ± 200	71.3	152.7	0.418 ± 0.014	0.376 ± 0.048

Note: The change in neutron lifetime for a change in solution height from 29.5 cm to a solution height of 7.3 cm was a factor of 2.1.

<sup>a</sup>Uncertainties are taken from Tables III and VI.

<sup>b</sup>Uncertainties are one standard deviation of the mean from the least-squares fitting of data.

<sup>c</sup>Average of values from Table V unperturbed by air bubbles.

<sup>d</sup>Assumed to be equal to the average value from the ratio of spectral densities.

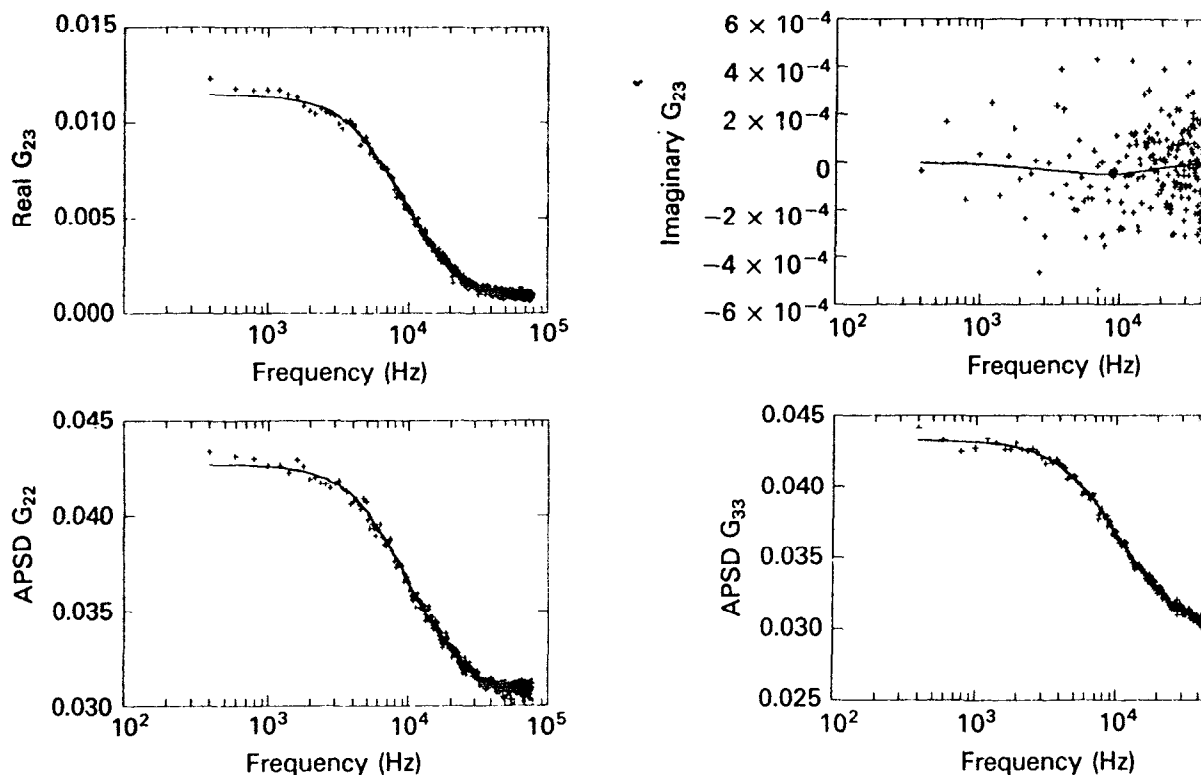


Fig. 9b. CPSD  $G_{23}$  and APSDs  $G_{23}$  and  $G_{33}$  as a function of frequency for a solution height of 13.1 cm v source on the bottom of the tank and the scintillators located as shown in Fig. 2. (Lines are fitted functions.)

fractions, are higher than those from the ratios of spectral densities. In previous experiments, the validity of the BFNA method was usually limited to  $k_{eff}$  values down to  $\sim 0.8$ .

### CONCLUSIONS

The results and conclusions of these experiments are as follows:

1. The capability to measure the subcriticality for a multiplying system to  $k_{eff}$  as low as 0.3 was demonstrated.
2. Experimental  $k_{eff}$  values were obtained from the ratio of spectral densities in times as short as 6 s of data accumulation, and a small fraction of a second analysis time as a solution tank was drained from a height of 29.5 to 6.5 cm in  $\sim 60$  s with corresponding changes in  $k_{eff}$  from 0.95 to 0.30.
3. The measured  $k_{eff}$  values obtained did not depend on the speed at which the solution height was changed or whether the tank was filling or draining.
4. The results of the dynamic measurements agreed with the static measurements.
5. Where static measurements were practical (limited to  $k_{eff}$  down to  $\sim 0.5$  by detection efficiency) with

$^3\text{He}$  proportional counters sensitive to neutron the results agreed with those from measurement scintillation detectors sensitive to gamma rays at trons.

6. As in previous experiments, the ratios of central densities at low frequency were used successfully to obtain  $k_{eff}$  values using a modified point kernel interpretation of the data.

7. The neutron multiplication factors from independent measurements using the BFNA method with the values of  $k_{eff}$  from the measured ratios of spectral densities down to  $k_{eff}$  values of 0.65.

8. The effectiveness of this method for systems where conditions are changing as demonstrated probably exceeds the dynamic requirements of most fuel plant processing applications.

9. Calculated  $k_{eff}$  values using the KENO Carlo code and Hansen-Roach cross sections compared well with the experimental values.

The demonstrated dynamic capability of this method down to neutron multiplication factors allows continuous monitoring of the criticality of process tanks or dissolvers and thus allows reduction of excess conservatism from plant design, leading

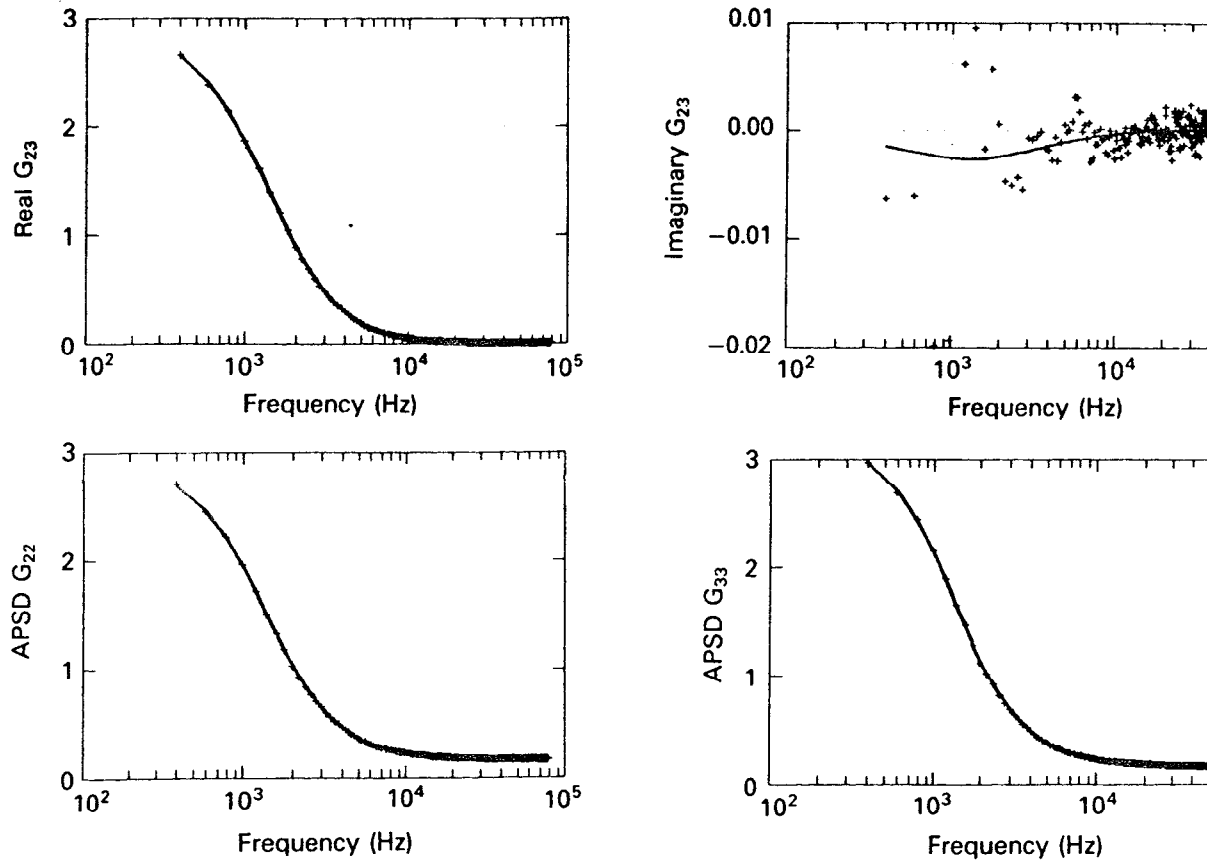


Fig. 9d. CPSD  $G_{23}$  and APSDs  $G_{22}$  and  $G_{33}$  as a function of frequency for a solution height of 29.5 cm v source on the bottom of the tank and the scintillators located as shown in Fig. 2. (Lines are fitted functions.)

for detectors 2 and 3 located outside the fissile material system, as well as the APSD of a detector [Eq. (A.2)], were derived previously using the Langevin equation approach<sup>14</sup> with the assumption that detector noise and reactor noise are not correlated<sup>2</sup>:

$$G_{11}(\omega) = 2|h_1(\omega)|^2 \left( \frac{31}{2} F_c \bar{q}_\alpha^2 + F_c \bar{q}_c^2 \right), \quad (\text{A.1})$$

$$G_{22}(\omega) = |h_2(\omega)|^2 \left[ 2W_2 F \bar{q}_2^2 + \frac{W_2^2 (\bar{q}_2)^2}{\bar{\nu}^2} |H_s(\omega)|^2 G_s \right], \quad (\text{A.2})$$

$$G_{12}(\omega) = 2h_1^*(\omega)h_2(\omega)\bar{q}_c \frac{W_2 \bar{q}_2}{\bar{\nu}} H_s(\omega) \frac{\bar{\nu}_c F_c I_c}{I}, \quad (\text{A.3})$$

and

$$G_{23}(\omega) = h_2^*(\omega)h_3(\omega) \frac{W_2 \bar{q}_2}{\bar{\nu}} \frac{W_3 \bar{q}_3}{\bar{\nu}} |H_s(\omega)|^2 G_s, \quad (\text{A.4})$$

where

$h_1(\omega), h_2(\omega), h_3(\omega)$   
= response of the electronic component of detection systems 1, 2, and 3, respectively, at frequency  $\omega$

$\bar{q}_c, \bar{q}_\alpha$  = average charge produced in detector per  $^{252}\text{Cf}$  spontaneous fission and average charge produced per alpha particle, respectively

$\bar{q}_2, \bar{q}_3$  = average charge produced per interaction in detectors 2 and 3, respectively

$W_2, W_3$  = detection efficiency of detection systems 2 and 3, expressed as counts per interaction per fission

$W_1$  = efficiency for detecting  $^{252}\text{Cf}$  fission neutrons, assumed to be  $\approx 1$

$G_s$  = APSD of the reactor noise-equivalent source

and an asterisk designates complex conjugation. Frequencies much larger than delayed neutron constants,

where

$$S_R^{-1} = \frac{\text{multiplication of all neutrons}}{\text{multiplication of californium neutrons}} \frac{1}{A}$$

$$= \frac{Y}{A} \quad (\text{A.8})$$

or

$$S_R^{-1} = \frac{F_c I_c \bar{\nu}_c + F_i I_i \bar{\nu}_i}{F_c I_c \bar{\nu}_c A} \quad (\text{A.9})$$

The factor  $Y$  accounts for the effect of fissions induced by neutrons from the inherent source contributing to  $G_{23}$  but not to  $G_{12}$  or  $G_{13}$ . If not all of the  $^{252}\text{Cf}$  fissions are counted in the detection system electronics, then the fraction of californium fissions counted  $A$  must be introduced into  $S_R$  to account for these undetected fissions of californium, producing neutrons that induce fissions in the system that contribute to  $G_{23}$  but not to  $G_{12}$  and  $G_{13}$ .

When a multiplying system is far subcritical, the power spectral density of the noise-equivalent source  $G_5$  must be modified to include  $X'$ , a modified form of the neutron dispersion number given by Eqs. (A.5) and (A.6). Then,  $(1 - k_{eff})/k_{eff}$  is of the form

$$\frac{1 - k_{eff}}{k_{eff}} = \frac{C_1 G_{12}^* G_{13} / G_{11} G_{23}}{1 - C_2 G_{12}^* G_{13} / G_{11} G_{23}} \quad (\text{A.10})$$

instead of

$$\frac{1 - k_{eff}}{k_{eff}} = C \frac{G_{12}^* G_{13}}{G_{11} G_{23}}, \quad (\text{A.11})$$

where  $C$ ,  $C_1$ , and  $C_2$  are constants involving parameters defined by Eqs. (A.1) through (A.11), some of which depend on solution height.

If it is assumed that reactor and detector noises are completely correlated,<sup>16,17</sup> the value of  $C_2$  is  $\bar{\nu}_c \cdot (\bar{\nu}_c - 1) / (\bar{\nu}_c)^2$  while the value of  $C_1$  is essentially the same. The sensitivity of the interpretation of the data to the assumption of complete correlation between detector and reactor noises is examined in Appendix B.

If spatial modal effects are significant, the ratio of spectral densities can be multiplied by a calculated spatial modal correction factor  $M_c$ , which is the ratio of  $G_{12}^* G_{13} / G_{11} G_{23}$ , obtained from fundamental mode only, to that obtained with all modes present. Since there is a modal correction factor  $M_{ij}$  for each CPSD  $G_{ij}$ , point kinetics interpretation of the data can yield valid results if the modal correction to the numerator is the same as that for the denominator (i.e.,  $M_{12} M_{13} / M_{23} = 1$ ). This factor can be calculated according to the methods of Verdu-Martin et al.<sup>18</sup> and Verdu-Martin<sup>19</sup> for unreflected cylindrical geometries. An alternate approach<sup>20,21</sup> is to fit the data to sums of modes if practical and obtain the fundamental mode ratio directly from the experimental data. In general, this separation of the fundamental mode ratio is not practical.

## APPENDIX B

### PARAMETERS FOR INTERPRETATION OF THE RATIO OF SPECTRAL DENSITIES TO OBTAIN THE NEUTRON MULTIPLICATION FACTOR AND SENSITIVITY STUDIES

Several parameters that appear in Eqs. (A.1) through (A.11) in Appendix A and are used for interpretation of the ratio of spectral densities to obtain the neutron multiplication factor can be independently measured or obtained from measurements of other parameters. The origins of these parameters and their values are described below. Also, the sensitivity of the interpretation to variations in these parameters is presented as a function of  $k_{eff}$  value.

The value of  $q_\alpha$  is zero. This results from the electronics associated with the  $^{252}\text{Cf}$  ionization chamber which discriminates against the contribution to the signal from alpha-particle decay in the ionization chamber. The value of  $q_c$  is unity because the contribution to the signal from all  $^{252}\text{Cf}$  fissions are the same.

Since there is no significant inherent neutron source in the uranyl nitrate solution comparable to the size of the  $^{252}\text{Cf}$  source, the third term in Eq. (A.1) is zero, and since >99.5% of the  $^{252}\text{Cf}$  spontaneous fission produces signals in channel 1 and these signals are counted,  $Y = A = S_R = 1$ .

The average number of neutrons per uranium fission was obtained by using the fluxes from transport theory calculations and the ENDF/B-IV data<sup>22</sup> to calculate the total number of neutrons per uranium fission. This averaging accounts properly for the dependence of the average number of neutrons per fission on the energy of the neutron inducing the fission. Changing solution height resulted in a <0.2% change in the value of the number of neutrons per fission, and the resulting average number of neutrons per uranium fission was 2.426. The value of the average number of prompt neutrons per fission  $\bar{\nu}$  is 2.408 and was used for interpretation at all solution heights.

The number of delayed neutrons per uranium fission was calculated from the delayed neutron yield and the delayed neutron effectiveness factors obtained by using the forward and adjoint fluxes from transport theory,<sup>23</sup> and the delayed neutron spectra of Batchelor and McKhyder.<sup>24</sup> The effective delayed neutron fraction calculated in this way is 0.0075.

The value of the Diven factor [ $X = \bar{\nu}(\bar{\nu} - 1)$ ] was obtained from the measurements of prompt neutron multiplicities for uranium. Its value does not depend significantly on the energy of the neutron inducing fission and varies only from 0.796 to 0.80 when the neutron energy varies from thermal to 2 MeV (Ref. 25). The value of  $X$  used was 0.80. The value of the number of prompt neutrons per  $^{252}\text{Cf}$  fission  $\bar{\nu}_c$  and its mean square  $(\bar{\nu}_c^2)$  are from the measurements of prompt neutron multiplicities of Speiser et al.,<sup>26</sup>  $\bar{\nu}_c = 3.773$  and  $\bar{\nu}_c^2 = 15.818$ .

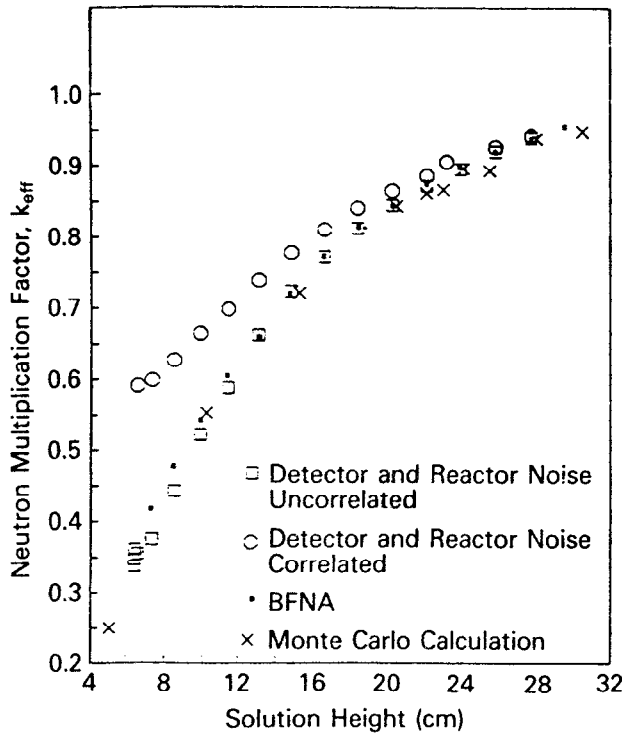


Fig. B1. Sensitivity of neutron multiplication factors to assumptions concerning correlation of reactor and detector noises.

yields  $k_{eff}$  values that differ from those for the uncorrelated assumption below 0.85, and the difference increases as  $k_{eff}$  decreases to as much as a factor of 2 at  $k_{eff} = 0.35$ . The results of the interpretation, assuming that reactor and detector noise are correlated, also differ from other measurements and calculations.

APPENDIX C

CALCULATED NEUTRON MULTIPLICATION FACTORS

The neutron multiplication factors were calculated using the Monte Carlo method with the KENO code and Hansen-Roach<sup>29</sup> and ENDF/B-IV cross section data. The calculations included the source and its Lexan tube and the reflection effect of the scintillation detector as located in the measurements. The results of the calculations are given in Table C.I. The small reaction effect of the detectors that cannot be reliably obtained from the calculations by subtracting the calculated neutron multiplication factors from calculations with a detector without the detector was included because of the statistical uncertainty of the calculations ( $\pm 0.005$ ). The  $k_{eff}$  values using the ENDF/B-IV data were consistently higher than those from Hansen-Roach cross sections by an average of 2% in  $k_{eff}$ . The calculated

TABLE C.I

Neutron Multiplication Factors from Monte Carlo Calculations with Hansen-Roach Cross Sections

Solution Height (cm)	Calculated Neutron Multiplication Factors <sup>a</sup>			
	Hansen-Roach Cross Sections			ENDF/B-IV 27 Group (No Source or Scintillators <sup>d</sup> )
	Source and Scintillators <sup>b</sup>	Source Only <sup>c</sup>	No Source or Scintillators <sup>d</sup>	
30.5	0.949	0.950	0.963	0.982
27.9	0.939	0.916	---	---
25.4	0.894	0.896	0.902	0.938
24.0	0.897	---	---	---
22.9	0.867	0.870	---	---
22.0	0.862	---	---	---
20.4	0.844	0.831	0.841	0.868
15.2	0.721	0.721	0.741	0.763
10.2	0.553	0.547	0.544	0.574
5.08	---	0.241	0.249	0.256

<sup>a</sup>Statistical error is  $\sim 0.005$ . All calculations included the bottom, sides, and top of the tank. Where the source was included in the calculation, the 2.54-cm-o.d. Lexan tube was included in the calculation. As a result, with the source located at any height of solution, the Lexan tube displaced solution on the axis of the cylinder above the source position.

<sup>b</sup>Source located at the bottom of the tank and the scintillators as shown in Fig. 2 were included in the calculation.

<sup>c</sup>Source at the center of solution height on the axis of the tank was included in the calculation.

<sup>d</sup>Source and scintillators were not included in the calculations.

R. A. Todd and M. S. Emery in the design and modification of the ADC system; of M. M. Chiles and V. C. Miller for the design, testing, and development of the high-efficiency scintillation detectors; of G. W. Allin in engineering support; and of C. E. Murphy for technical assistance. For the use of the  $^{252}\text{Cf}$ , the authors are indebted to the DOE Office of Basic Energy Sciences, Division of Chemical Sciences, through the transplutonium element production facilities at ORNL. The authors acknowledge the support of PNC and DOE through the Consolidated Fuel Reprocessing Program at ORNL. The thorough review of this report by H. Funabashi of PNC is gratefully acknowledged.

This research was sponsored by the Office of Facilities, Fuel Cycle, and Test Programs, DOE, under contract No. DE-AC05-84OR21400 with Martin Marietta Energy Systems and PNC of Japan. The ORNL is operated by Martin Marietta Energy Systems for the DOE.

#### REFERENCES

1. J. T. MIHALCZO, V. K. PARÉ, G. L. RAGAN, M. V. MATHIS, and G. C. TILLET, *Nucl. Sci. Eng.*, **66**, 29 (1978).
2. J. T. MIHALCZO, W. T. KING, and E. D. BLAKEMAN, " $^{252}\text{Cf}$ -Source-Driven Neutron Noise Analysis Method," presented at Workshop on Subcriticality Reactivity Measurements, Albuquerque, New Mexico, August 1985, CONF-8508105.
3. Memorandum of Agreement between the U.S. Department of Energy and the Power Reactor and Nuclear Fuel Development Corporation, Japan, in the area of Criticality Data Development, signed August 12, 1983.
4. W. T. KING, J. T. MIHALCZO, and E. D. BLAKEMAN, *Trans. Am. Nucl. Soc.*, **47**, 239 (1984).
5. J. T. MIHALCZO and W. T. KING, *Trans. Am. Nucl. Soc.*, **43**, 408 (1982).
6. J. T. MIHALCZO and W. T. KING, *Nucl. Technol.*, **84**, 205 (1989).
7. J. T. MIHALCZO, W. T. KING, and E. D. BLAKEMAN, *Trans. Am. Nucl. Soc.*, **49**, 241 (1985).
8. J. T. MIHALCZO, E. D. BLAKEMAN, and W. T. KING, *Trans. Am. Nucl. Soc.*, **52**, 640 (1986).
9. J. T. MIHALCZO, W. T. KING, and E. D. BLAKEMAN, *Trans. Am. Nucl. Soc.*, **50**, 307 (1985).
10. W. T. KING and J. T. MIHALCZO, *Trans. Am. Nucl. Soc.*, **33**, 796 (1979).
11. J. T. MIHALCZO, W. T. KING, E. B. JOHNSON, and E. D. BLAKEMAN, *Trans. Am. Nucl. Soc.*, **45**, 337 (1983).
12. M. V. MATHIS, J. T. DeLORENZO, M. M. CHILES, and J. T. MIHALCZO, "Nuclear Detection Instrumentation for Reactivity Measurements with the Fast Flux Test Facility Engineering Mockup Core," *IEEE Trans. Nucl. Sci.*, **NS-22**, 691 (1975).
13. C. W. RICKER, D. N. FRYY, E. R. MANHANAUER, "Investigation of Negative Reactivity Measurement by Neutron Fluctuation Analysis," *Noise Analysis in Nuclear Systems*, Gainesville, November 1963.
14. P. LANGEVIN, *Acad. Sci. Paris CR*, **46**.
15. C. E. COHN, *Nucl. Sci. Eng.*, **7**, 472 (1959).
16. Y. YAMANE, S. WATANABE, K. NIIMIYOSHI, T. SUZAKI, and I. KOBAYASHI, *Ergy Soc. Jpn.*, **28**, 9, 850 (1986).
17. F. C. DIFILIPPO, *Nucl. Sci. Eng.*, **99**, 2.
18. G. VERDU-MARTIN, J. L. MUÑOZ-CAMACHO, and W. T. KING, *Trans. Am. Nucl. Soc.*, **46**, 452 (1984).
19. G. VERDU-MARTIN, "Teoría General de Estocástico de Neutrones y su Aplicación a la Reactividad en Conjuntos Subcríticos," Thesis, Politecnica de Valencia (Apr. 1984).
20. C. MARCH-LEUBA, "Interpretation of Reactivity Measurement with Strong Spatial Effects," Thesis, University of Tennessee (1987).
21. C. MARCH-LEUBA, J. MARCH-LEUBA, and F. C. DIFILIPPO, *Trans. Am. Nucl. Soc.*, **54**, 348 (1987).
22. G. D. GARBER, "ENDF-7-201, ENDF/E-7-201 Documentation," BNL-17541, Brookhaven National Laboratory (1975).
23. W. A. RHOADES, D. B. SIMPSON, R. L. BROWN, and W. W. ENGLE, Jr., "The DOT-IV Two-Dimensional Discrete Ordinates Transport Code with Space-Mesh and Quadrature," ORNL/TM-6529, Oak Ridge National Laboratory (1979).
24. R. BATCHELOR and H. R. MCKHYDE, *Energy*, **3**, 7 (1956).
25. M. S. ZUCKER and N. E. HOLDEN, *Trans. Am. Nucl. Soc.*, **52**, 636 (1986).
26. R. R. SPENCER, R. GWINN, and R. INCROPERA, *Sci. Eng.*, **80**, 603 (1982).
27. L. M. PETRIE and N. F. CROSS, "KENO-Improved Monte Carlo Criticality Program with Singularity," ORNL/NUREG/CSD-2, Vol. 2, Oak Ridge National Laboratory (1985).
28. L. M. PETRIE and N. F. CROSS, "KENO-Improved Monte Carlo Criticality Program," Oak Ridge National Laboratory (1975).
29. G. E. HANSEN and W. H. ROACH, "Six-Group Cross Sections for Fast and Intermediate Energy Assemblies," LAMS-2543, Los Alamos Scientific Center (1961).